Probe of the excitonic transitions and lifetimes in quasi-2D organic–inorganic halide perovskites

Cite as: AIP Advances 12, 015114 (2022); doi: 10.1063/5.0072566
Submitted: 23 September 2021 • Accepted: 17 December 2021 •
Published Online: 10 January 2022

Brenden A. Magill,[1] Kai Wang,[2,3] Stephen McGill,[4] Christopher J. Stanton,[5] Shashank Priya,[2,3] and Giti A. Khodaparast[1,a)]

AFFILIATIONS

[1] Department of Physics, Virginia Tech, Blacksburg, Virginia 24061, USA
[2] Bio-inspired Materials and Devices Laboratory (BMDL), Center for Energy Harvesting Materials and Systems (CEHMS), Virginia Tech, Blacksburg, Virginia 24061, USA
[3] Materials Research Institute, Penn State, University Park, Pennsylvania 16802, USA
[4] National High Magnetic Field Laboratory, Tallahassee, Florida 32310, USA
[5] Department of Physics, University of Florida, Gainesville, Florida 32611, USA

[a)] **Author to whom correspondence should be addressed:** khoda@vt.edu

ABSTRACT

Traditional organic–inorganic halide perovskites (OIHPs), in which perovskites layers are separated by an organic spacer material, have been mainly explored for photovoltaics devices, but they also offer promises for nonlinear optics and quantum light applications. These attributes include (a) high quantum efficiency, (b) large binding energy of excitons in low-dimensional structures, (c) polarons of long coherence times at room temperature, and (d) a large spin–orbit coupling. OIHP systems can be engineered to have photoluminescence (PL) emissions from UV to IR regions, in addition to power conversion efficiencies, in excess of 24%. This class of materials offers broad tunability of its properties, through controlling the number of atomic layers in the quantum well, tuning the organic spacer thickness, or even engineering the composition with exotic dopants. In this work, we present PL and time-resolved PL measurements of quasi-2D BA_2PbI_4 and provide new insights on the temperature dependence of their excitonic dynamics and fine structures of their PL emissions. We observed long lifetimes, which can result from the formation of large polarons, screening the Coulomb interactions of the charge carriers and reducing the scattering of the carriers with charge defects.

I. INTRODUCTION

Organic–inorganic halide perovskites (OIHPs) are an exciting new class of multifunctional materials and can be employed toward the development of highly sensitive detectors in multiple optical ranges, such as visible,[1,2] x ray,[3,4] gamma ray,[5] and THz,[6] as well as light sources, such as light-emitting diodes,[7–9] THz emitters,[6] and lasers.[10] Specifically, the excitonic properties in these materials are important to understand, so they can be utilized to tune and enhance their optical emission to create next-generation light sources.[11] In addition, they have been proposed for neuromorphic computing,[12,13] not to mention the widespread interest in these materials for photovoltaic devices.[14–16] Unfortunately, stability issues in these materials, when in bulk (3D), can limit their applications in the development of devices.[9,14,16] However, it has been shown that reducing the dimensionality can improve material stability as well as creating new functionalities in these materials.[15,17,18] Additionally, layered perovskites are considered qualitatively to be similar to quantum wells (QWs), but this assumption has failed to capture many of their properties,[19] driving motivations for further research, especially in understanding the optical properties of quasi-2D systems.

These materials can be engineered to have a strikingly diverse assortment of optical properties by partitioning sheets of halide perovskites (HPs) between cation layers, typically organic molecules, to create quasi-2D materials. For example, photoluminescence (PL) emission, from layered organic–inorganic perovskites, covers a broad range from red to near-UV, with spectral widths for those emissions that can vary between covering the whole visual spectrum (400–700 nm)[17,20–23] (typically referred to as broadband or white light emission), to narrow lines, with full width at half maximum (FWHM) of less than 100 meV.[17,23] The possibility of having broad wavelength emissions and spectral widths has prompted intensive investigations of these hybrid organic–inorganic materials, to understand their material properties with eyes on implementing them into next-generation devices.[2,24]

$BA_2MA_{n-1}Pb_nI_{3n+1}$ is currently of interest for the creation of blue and white light-emitting LEDs but suffers from a low quantum efficiency.[25] The source of this low quantum efficiency is not well understood[23] but could be due to strong exciton–phonon coupling in single-layer quasi-2D HPs[26] or possibly traps and defects. In this study, we present new experimental observations to probe the excitonic coupling in $BA_2MA_{n-1}Pb_nI_{3n+1}$, where we performed measurements of PL and time-resolved photoluminescence (TRPL), at temperatures below 100 K.

II. METHODS

Our quasi-2D perovskites of $BA_2MA_{n-1}Pb_nI_{3n+1}$ were synthesized from aqueous solutions, according to the water–air interface method. Lead(II) oxide was first dissolved in a mixture of hydroiodic acid (5 ml) and hypophosphorous acid solution (850 μl) and heated up to 100°C producing a pale-yellow solution. Different molar ratios of MACl and BA were slowly added into another vial containing 3 ml of hydroiodic acid in an ice-water bath. After a transparent solution was obtained upon heating, the alkylammonium precursor solution was slowly added into the lead solution under magnetic stirring, producing a transparent yellow solution at elevated temperature. Specifically, for our n = 1 samples, the precursor ratio is PbO powder (2232 mg, 10 mmol), HI solution (10.0 ml, 76 mmol), n-$CH_3(CH_2)_3NH_2$ (924 μl, 10 mmol), and HI 57% w/w (5 ml, 38 mmol). The crystallization first occurs at the water–air interface followed by a fast-lateral growth within the water–air plane. The flake with an area of centimeter-scale is typically increased within 1 min to half an hour depending upon the molar ratio between methylammonium and butylammonium. The whole process was carried out in ambient conditions, and the crystal was dried overnight in a vacuum oven at 40 °C.

As shown in Fig. 1, the XRD pattern of the single-crystalline sample was obtained from a Philips Xpert -Pro X-ray diffractometer (Almelo, The Netherlands) with Cu Ka radiation. Furthermore, Fig. 2(a) presents the layers in our sample with the B-site being Pb. Our BA_2PbI_4 sample exhibited a bright emission clearly visible to the naked eye, at a low excitation power of 100 μW, as shown in Fig. 2(b).

In this study, we monitored the PL emissions from 1.6 to 100 K where these measurements were performed in a flow-through cryostat. The laser excitation source was a Ti:sapphire oscillator with an 80 MHz repetition rate. Furthermore, the pulses were upconverted to 400 nm using a nonlinear β-barium borate (BBO) crystal, with a dichroic filter used after the crystal, to separate the 400 nm

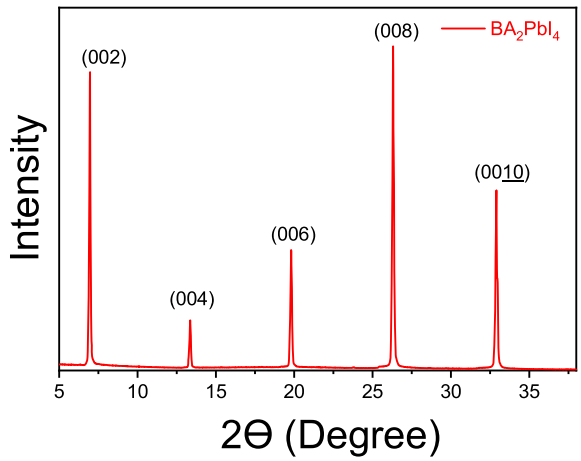

FIG. 1. X ray diffraction (XRD) pattern of the BA_2PbI_4 single-crystalline flake.

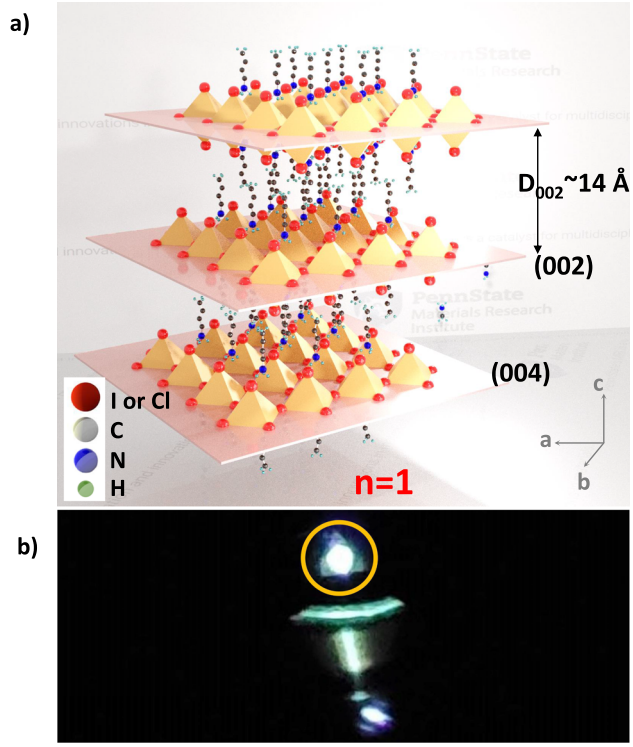

FIG. 2. (a) Layer structure of $BA_2MA_{n-1}Pb_nI_{3n+1}$ at room temperature. In our sample, the A-site being the BA+ (organic spacer), B-site being Pb^{2+}, and X-site being the I^-. Here, n = 1 suggests a mono octahedral layer inserted between organic spacer, which is in a strict 2D structure. (b) BA_2PbI_4 displayed, a clearly visible to the naked eye emission, as shown in the photo taken through the cryostat's window. The sample was excited at 400 nm with an average power of 100 μW, while kept at 100 K. The PL from the sample is circled in yellow and the other images are the reflections from the sample holder and the rings around the cryostat's window.

pulses from the 800 nm pulses. To explore the dynamical response in this material system, we employed TRPL, for temperatures ranging from 1.6 to 100 K. Light emitted from the sample, in a reflectivity geometry, was collected using an avalanche photodiode. A time-correlated single-photon counting system (Picoharp 300) was used for the time-resolved measurements. We should note, neither PL nor TRPL showed any strong magnetic field dependence, by tuning the external fields up to 10 T, and we are not presenting the data here.

III. RESULTS AND DISCUSSION

The PL emissions in quasi-2D OIHPs have been previously attributed to a combination of emissions from free and bound excitons, trap states, and the organic layers.[21,27–30] In the inorganic layers, the origin of PL has been attributed to radiative recombination of excitons that migrate freely in the lattice (free excitons), excitons that are pinned by lattice defects, or due to excitons creating transient lattice deformations that trap them (self-trapped excitons).[28–30] In previous studies,[28,31] excitonic emission has been identified as the primary source of PL in these materials, with the carrier–carrier (*i.e.,* exciton continuum) band edge recombination, to be absent. In the case of the organic layers, the origin of the PL emissions has been attributed to the energy transfer in the inorganic layers as well as directly from chromophores in the organic layer.[27,32] Additionally, these simultaneous pathways can result in multiple possibilities, including free and trapped exciton recombination or emissions, from both the organic and inorganic layers.

In an earlier study on lead-based OIHPs, a similar pattern with two broad and two narrow peaks has been modeled to be due to emissions from two competing lattices,[20] resulting from an incomplete phase transition. BA_2PbI_4 is in a tetragonal phase at room temperature and starts but does not complete a transition to an orthorhombic phase when the temperature is reduced,[33,34] similar to other lead-based HPs.[35]

In a study by Wu *et al.*,[20] the identified narrow features were attributed to free excitons and the observed broader features, to bound excitons in the tetragonal and orthogonal phases, respectively. Alternatively, this could be due to the band edge and higher-order excitons.[28] In similar lead-based HPs, the observed broad features have been attributed to trapping states;[17,20] however, the origin of the observations varies considerably.[36]

In Fig. 3(a), we present the PL from BA_2PbI_4, excited using an incident power of 100 μW at 400 nm. The PL displays two sharp peaks and two broader peaks, and at temperatures under 40 K, small satellite peaks around the features above 2.3 eV. The intensity of the PL spectra in Fig. 3(a) increases as the temperature decreases. We show the spectra taken at 1.6 K, as shown in Fig. 3(b) on a smaller energy scale so we can focus on the small features that appear around the main peaks (P_1–P_3), at low temperature. These features are likely exciton complexes bound to shallow donor and acceptor impurities (either neutral or charged), with P_1–P_3 bound to shallower levels and P_4 bound to a broader distribution of deeper level impurities.[37] We should note for the peak P_1, we observed a small increase (approximately 20% on a linear scale) in the PL intensity at 10 T.

The origin of the PL in OIHPs is assumed to be due to excitonic emission.[21,27–29] As such, we can estimate the binding energy of an

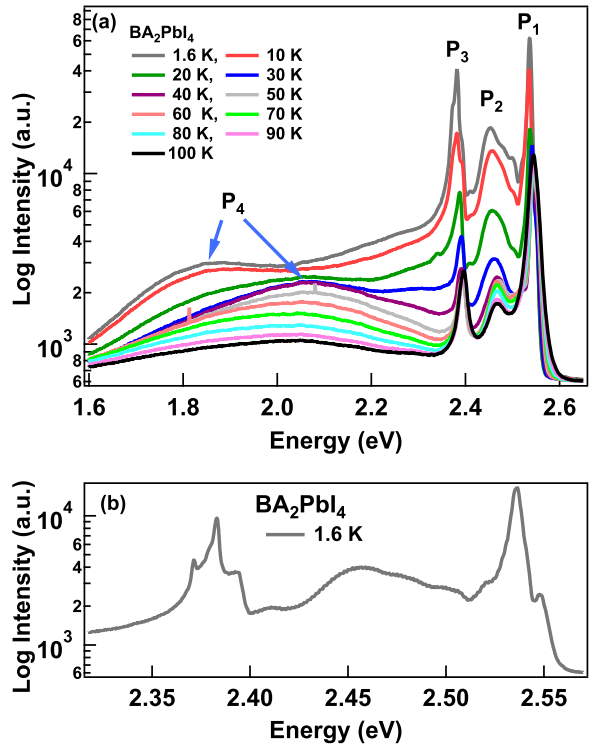

FIG. 3. (a) PL response for BA_2PbI_4, from 1.6 to 100 K, displaying a complicated multi-peak structure. With the principle emission peaks labeled P_1–P_4. (b) Close up of the 1.6 K trace displaying the complicated structures of P_1–P_3.

exciton by examining the emission intensity as a function of temperature using its relaxation rate, $k_{ex} = k_r + k_{nr}$, where k_r and k_{nr} are the radiative and non-radiative decay constants.[38] Then, we can separate the non-radiative term into a thermally activated $k^*_{\mathrm{dis}}\exp(-E_b/k_bT)$ (with E_b being the exciton binding energy) which arises from exciton dissociation, and $k_{onr}(T)$ for other non-radiative processes, such as Shockley–Reed–Hall (SRH), and Auger recombination. Therefore, we can write

$$k_{ex} = k_r + k_{onr}(T) + k_{dis}\exp\left(-\frac{E_b}{k_bT}\right), \tag{1}$$

where k_b is the Boltzmann constant. Among these, k_{dis} has been shown to be the principle source of non-radiative recombination while other sources of non-radiative recombination only contribute weekly to the recombination rate.[38,39] Therefore, we can disregard the non-exciton non-radiative relaxation term. The emission quantum yield is given by k_r/k_{ex}; therefore, we can express the inverse of the quantum yield of the PL, $1/\Phi(T)$ as a function of temperature in the following equation:

$$\frac{1}{\Phi(T)} = \frac{1}{\Phi(T=0)} + \frac{k_{dis}}{k_r}\exp\left(-\frac{E_b}{k_BT}\right). \tag{2}$$

If we assume that the dominant component of the PL emission is excitonic, then we can express the inverse of the emission intensity

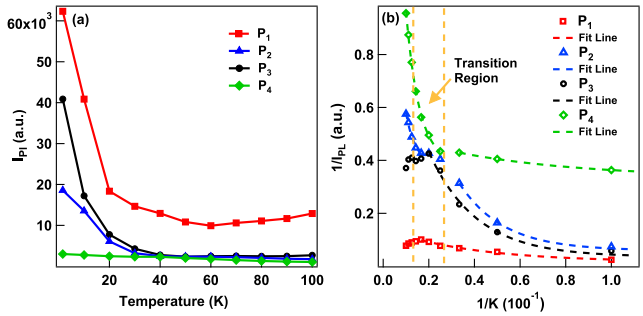

FIG. 4. (a) Intensity of the PL peaks in Fig. 3(a) as a function of temperature. (b) Inverse peak intensity, displaying fits of each peak for extracting the exciton binding energy, as described in the text. The orange-dashed lines are indicating the transition regions for $1/I_{PL}$.

$I(T)$ as

$$\frac{1}{I(T)} = A + B\exp\left(-\frac{E_b}{k_B T}\right), \tag{3}$$

where A and B are fitting parameters that correspond to the inverse of the emission intensity at T= 0 K and k_{dis}/k_r, respectively. Thus, we can employ Eq. (3) to extract fits for the exciton binding energies in our sample. In addition, if we cannot fit the PL intensity with a simple exponential decay, at different temperatures, this tells us that the origin of the excitonic emission is more complicated and may have additional components, such as phonon replicas or multiple impurity states.

In Fig. 4(a), we present the intensity of all of the peaks as a function of temperature. It is notable that the intensity for both P_1 and P_3 decreases with temperature until 60 K, followed by an increase when reducing temperature. This observation suggests that the origin of the emission is not purely excitonic for temperatures above 60 K. This fact can be seen even more clearly in Fig. 4(b), where we plot the inverse of the intensity as a function of the inverse temperature, in addition to the fits using Eq. (3), in order to extract the exciton binding energies. In Table I, we present the binding energies extracted from our fits in Fig. 4(b), where E_{b1} is the fit for temperatures below 25 K and E_{b2}, for above 40 K.

As can be seen in Fig. 4(b), there appear to be two temperature regimes that display different exciton binding energies. These two temperature regions are above 40 K and below 25 K. Above 40 K, the behavior of P_1 and P_3 are both non-excitonic but, on the other hand, P_2 and P_4 both display excitonic behavior. Below 25 K, all four peaks are well modeled using an exponential decay, but the binding energies extracted, using Eq. (3) (presented in Table I) for the low-temperature regime are quite small compared to the previously observed exciton binding energies. In fact, the energies we extract in the low-temperature range are more on the order of the LO phonon energies, that have been reported in bulk $MAPbI_3$,[40] suggesting that in this range the excitonic decays are phonon-assisted.

TABLE I. The extracted binding energies from Fig. 4(b).

Assigned PL Peaks	E_{b1} (meV)	E_{b2} (meV)
P_1	23.2	...
P_2	45.4	210
P_3	41.0	...
P_4	15.4	149

Our results demonstrate the agreement of the excitonic binding energy from BA_2PbI_4, with the largest fit value (210 meV) compared to the previously measured value of 220 meV,[41,42] in this material. Lower E_{b1} values are more in line with the binding energies modeled in the bulk version of this material; $MAPbI_3$ (15–40 MeV),[43,44] or reported values for LO phonon energies (11–15 meV) for this structure.[40] Suggesting that there is either significant phonon-assisted decay occurring in this temperature range or the material is acting more like a bulk instead of single-layer material. The dramatic difference in the extracted fits in the low- and high-temperature regions suggests that the nature of the excitonic binding or the exciton phonon interaction energy changes dramatically between 25 and 40 K. It is useful to note that in similar materials, the binding energies of free excitons decrease as the temperature is decreased.[45,46] This fact leads to the location of the exciton emission peaks decreasing in energy, suggesting that peaks P_1–P_3 are likely bound exciton complexes (excitons under the band edge energy) associated with shallow donors and acceptors (both neutral and charge). The broad feature, labeled P_4 in our PL, is more likely due to excitons bound to a broader distribution of deeper impurity states.

We also report a transition, in the temperature dependence of the PL peak positions, in Figs. 5(a)–5(d) similar to what we observed in terms of the peak intensities of Fig. 4(b). In Figs. 5(a)–5(d), we present the peak positions in (energy) for P_1–P_4 and the trap states, as a function of temperature. As shown in Fig. 5(a), the position of P_1 initially increases in energy from 100 to 70 K, then decreases in energy, as the temperature decreases, with a sharper drop between 40 and 25 K, followed by a slight increase in energy at 1.6 K. In Fig. 5(b), we observe that the position of P_2 decreases

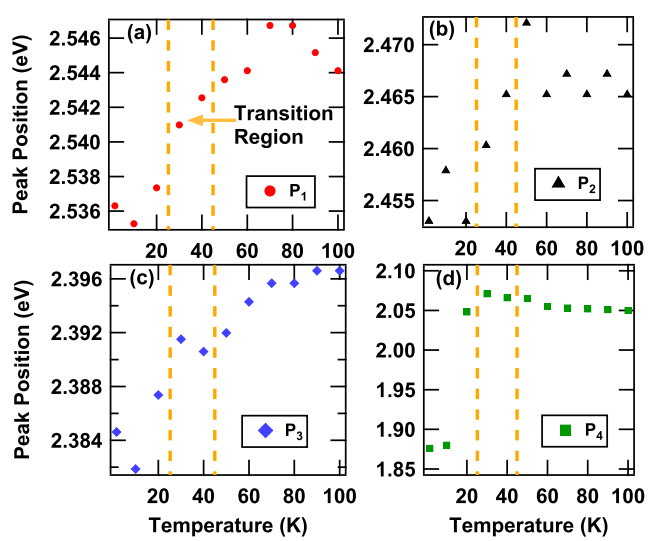

FIG. 5. Exciton peak positions in energy from Fig. 3(a) for all the principle features; P_1–P_4 are presented in panels (a)–(d), respectively. The dashed orange lines, in each panel, bound the regions in which the temperature dependence behavior changes.

slowly in energy from 100 to 50 K, then decreases more rapidly with temperature. As shown in Fig. 5(c), the behavior of P_3 is similar to that of P_1 and P_2, with the peak position decreasing in energy, as the temperature is decreased. In Fig. 5(d), we present the position of P_4 that, unlike the other peaks, initially increases in energy; as the temperature is decreased from 100 to 45 K, then decreases in position between 25 and 45 K.

It is known that in semiconductor materials, the exciton–phonon coupling can be examined through the temperature dependent broadening of the PL.[47,48] We can apply the same approach to our OIHP structure to explore the coupling between excitons and phonons. The linewidth of an excitonic emission can be characterized as[40,49]

$$\Gamma(T) = \Gamma_0 + \Gamma_{ac} + \Gamma_{LO} + \Gamma_{imp} = \Gamma_0 + \gamma_{ac}(T) + \gamma_{LO}N_{LO}(T) + \gamma_{imp}e^{-\frac{E_b}{k_BT}}, \quad (4)$$

where Γ_0, Γ_{ac}, Γ_{LO}, and Γ_{imp} represent the broadening due to the temperature-independent homogeneous term, the acoustic phonon coupling, the LO phonon coupling, and the impurity broadening, respectively. Additionally, the electron–phonon coupling is proportional to the occupation number of the phones, and $N_{LO}(T)$ is determined by the Bose–Einstein distribution,

$$N_{LO}(T) = \frac{1}{e^{E_{LO}/k_BT} - 1}, \quad (5)$$

where E_{LO} is the LO phonon energy.

In Fig. 6(a), we present the result of our fits to extract the FWHM as a function of temperature. An example of how we performed our fits is shown in Fig. 6(b) for the data at 10 K. We observe the FWHM of P_1 and P_3 decrease with temperature rather than reaching a plateau, which could be expected for an exciton in these materials.[46] In comparison, the FWHM of P_2 initially decreases then plateaus, and increases below 45 K. A simple exciton model, such as the one in Eq. (4), cannot describe the shape of P_2, but OIHPs with similar structures and different metal ions have displayed a FWHM with similar dynamics.[40] In these materials systems, the low-temperature behavior is attributed to the Fröhlich coupling between the free charge carriers and LO phonons.[40] The shape of our P_2 also changes as the temperature is decreased, and initially can be described by a Gaussian fit and then below 40 K, it can be better modeled using a Voigt fit.

These changes were occurring simultaneously after 30 K, suggesting that P_2 could be sensitive to some structural changes in our sample occurring at 30 K, similar to the observed variations of FWHM in HPs, when they experienced a transition between structural phases.[40] It is notable that the small sub-peaks in Fig. 3(a) are more predominantly resolved at temperatures below 30 K but do not demonstrate strong variation in energy or linewidth. These reported sharp features could be due to the fine structure splitting (*i.e.*, excited exciton states such as 2s, 2p, *etc.*) in the excitons, similar to what has been observed in Cs-based HPs.[46] or perhaps to different exciton-shallow impurity complexes, *i.e.*, neutral and charged donors and acceptors [cf. Ref. 37, page 347—Fig. 14.2(a) for Na]. In a similar temperature range, our sample displayed much sharper and better-resolved features compared to studies by Gelaz-Rueda *et al.*,[50] suggesting lower disorders in our system.

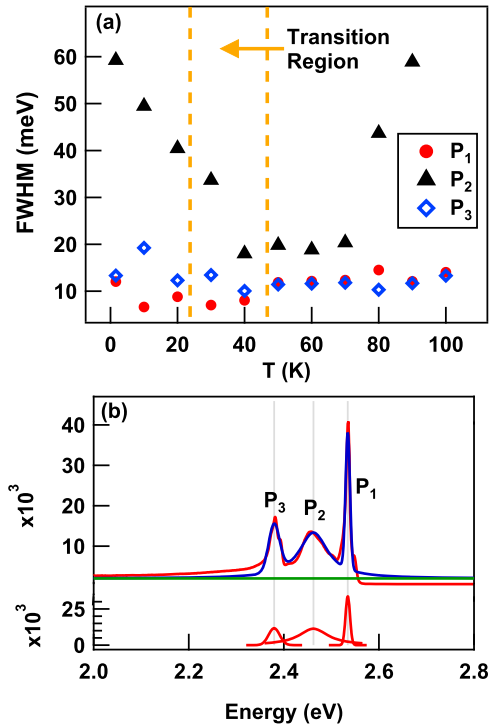

FIG. 6. (a) Observed FWHM for P_1, P_2, and P_3 as a function of temperature, with the orange-dashed lines, bounding the region in which the temperature dependence of the peak position, from Fig. 3(a), goes through a transition. (b) Here, we show an example of our fits for the measurement at 10 K.

In Fig. 7(a), we present TRPL for BA_2PbI_4, measured with an excitation wavelength of 384 nm and an incident power of 85 μW. We should note that Fig. 7(a) presents our TRPL results normalized to the trace with the highest intensity, as a function of temperature from 2 to 100 K, in a semi-log scale. The nature of our observation represents a dynamical response, wherein our measured time scale does not go to zero; therefore, in the semi-log scale, the traces

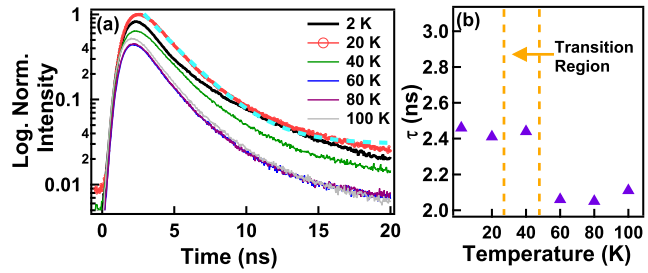

FIG. 7. TRPL measurements for BA_2PbI_4 (a) for temperatures between 2 and 100 K, normalized to the trace with the highest intensity, where the dashed line gives an example of the fit. (b) The time constant is associated with the initial relaxation part of the TRPL (τ) as a function of temperature. The orange lines are displaying the same temperature range that we observed transitional behavior in the PL, summarized in Fig. 5.

do not display a purely linear behavior. To extract the initial relaxation time scale (τ), we focused on the dynamical response below 20 ns, using a single exponential fit, and the results are summarized in Fig. 7(b), where we observed a sharp change in τ between 20 and 40 K, in a similar range where we observed the variation in the temperature dependence of the PL intensity, as well as the variation of the FWHM. These facts suggest that we are observing some fundamental changes in the emission mechanisms as well as the nature of excitonic emissions, in a narrow temperature range (20–40 K).

IV. CONCLUSION

In conclusion, we have explored the rich excitonic behavior of the PL in a quasi-2D organic–inorganic halide perovskite, BA_2PbI_4 over a broad temperature range, varying from 100 K down to 1.6 K. Our refinement and growth methods allowed us to resolve finer features in the luminescence spectrum compared to previous studies. We observed significant temperature dependence in our emission characteristics, including the PL's peak positions, the intensity of the individual peaks, and their widths. The observed transitions between 25 and 40 K suggest a sudden change either in the sample's structure or in the behavior of the excitons; likely due to a change in the LO phonon exciton coupling or the structural changes originating from the incomplete phase transition. We also observed significant temperature dependence in the excitonic lifetime. Our observed long lifetimes can be attributed to the formation of large polarons, in which these polarons can screen the Coulomb interactions of the charge carriers, thus reducing the scattering of the carriers with charge defects.

Above 40 K, we extracted exciton binding energies ranging from 149 to 210 meV, comparable to the 220 meV that has been reported in this material at higher temperatures.[41,42] Below 25 K, we report much lower binding energies for the excitons, on the order of the LO phonon energies (11–15 meV).[40] This fact might indicate that there is a phonon-assisted emission occurring in this region. We should note that bulk $MAPbI_3$ has exciton binding energies (15–40 meV) below 25 K, so it is also possible that at low temperatures, this material is behaving more like a bulk and less like a two-dimensional material.[43,44]

ACKNOWLEDGMENTS

This work was supported by the Air Force Office of Scientific Research under Award No. FA9550-17-1-0341 and DURIP funding (Grant No. FA9550-16-1-0358). A portion of this work was performed at the National High Magnetic Field Laboratory, which is supported by the National Science Foundation Cooperative Agreement No. DMR-1644779 and the State of Florida. G. A. Khodaparast acknowledges the support from L.C. Hassinger Faculty Fellowship.

AUTHOR DECLARATIONS

Conflict of Interest

The authors have no conflict of interest.

DATA AVAILABILITY

The data that support the findings of this study are available from the corresponding author upon reasonable request.

REFERENCES

[1] H. Wang and D. H. Kim, "Perovskite-based photodetectors: Materials and devices," Chem. Soc. Rev. **46**, 5204–5236 (2017).
[2] R. Dong, C. Lan, F. Li, S. Yip, and J. C. Ho, "Incorporating mixed cations in quasi-2D perovskites for high-performance and flexible photodetectors," Nanoscale Horiz. **4**, 1342–1352 (2019).
[3] W. Pan, H. Wu, J. Luo, Z. Deng, C. Ge, C. Chen, X. Jiang, W.-J. Yin, G. Niu, L. Zhu, L. Yin, Y. Zhou, Q. Xie, X. Ke, M. Sui, and J. Tang, "$Cs_2AgBiBr_6$ single-crystal X-ray detectors with a low detection limit," Nat. Photonics **11**(11), 726–732 (2017).
[4] A. J. Rowlands, "Material change for X-ray detectors," Nature **550**(7674), 47–48 (2017).
[5] H. Wei, D. DeSantis, W. Wei, Y. Deng, D. Guo, T. J. Savenije, L. Cao, and J. Huang, "Dopant compensation in alloyed $CH_3NH_3PbBr_{3-x}Cl_x$ perovskite single crystals for gamma-ray spectroscopy," Nat. Mater. **16**(8), 826–833 (2017).
[6] M. Manjappa, Y. K. Srivastava, A. Solanki, A. Kumar, T. C. Sum, and R. Singh, "Hybrid lead halide perovskites for ultrasensitive photoactive switching in terahertz metamaterial devices," Adv. Mater. **29**(32), 1605881 (2017).
[7] H. Cho, Y.-H. Kim, C. Wolf, H.-D. Lee, and T.-W. Lee, "Improving the stability of metal halide perovskite materials and light-emitting diodes," Adv. Mater. **30**(42), 1704587 (2018).
[8] J. Byun, H. Cho, C. Wolf, M. Jang, A. Sadhanala, R. H. Friend, H. Yang, and T.-W. Lee, "Efficient visible quasi-2D perovskite light-emitting diodes," Adv. Mater. **28**(34), 7515–7520 (2016).
[9] M. You, H. Wang, F. Cao, C. Zhang, T. Zhang, L. Kong, L. Wang, D. Zhao, J. Zhang, and X. Yang, "Improving efficiency and stability in quasi-2D perovskite light-emitting diodes by a multifunctional LiF interlayer," ACS Appl. Mater. Interfaces **12**(38), 43018–43023 (2020).
[10] P. Liu, X. He, J. Ren, Q. Liao, J. Yao, and H. Fu, "Organic–inorganic hybrid perovskite nanowire laser arrays," ACS Nano **11**(6), 5766–5773 (2017).
[11] T. Thu Ha Do, A. G. del Águila, D. Zhang, J. Xing, S. Liu, M. A. Prosnikov, W. Gao, K. Chang, P. C. M. Christianen, Q. Xiong, and Q. Xiong, "Bright exciton fine-structure in two-dimensional lead halide perovskites," Nano Lett. **20**(7), 5141–5148 (2020).
[12] P. C. Harikesh, B. Febriansyah, R. A. John, and N. Mathews, "Hybrid organic–inorganic halide perovskites for scaled-in neuromorphic devices," MRS Bull. **45**(8), 641–648 (2020).
[13] B. Ku, B. Koo, A. S. Sokolov, M. J. Ko, and C. Choi, "Two-terminal artificial synapse with hybrid organic–inorganic perovskite $(CH_3NH_3)PbI_3$ and low operating power energy (~47 fJ/μm^2)," J. Alloys Compd. **833**, 155064 (2020).
[14] G. Niu, X. Guo, and L. Wang, "Review of recent progress in chemical stability of perovskite solar cells," J. Mater. Chem. A **3**, 8970–8980 (2015).
[15] K. Wang, D. Yang, C. Wu, M. Sanghadasa, and S. Priya, "Recent progress in fundamental understanding of halide perovskite semiconductors," Prog. Mater. Sci. **106**, 100580 (2019).
[16] C. C. Boyd, R. Cheacharoen, T. Leijtens, and M. D. McGehee, "Understanding degradation mechanisms and improving stability of perovskite photovoltaics," Chem. Rev. **119**(5), 3418–3451 (2019).
[17] N. Wang, L. Cheng, R. Ge, S. Zhang, Y. Miao, W. Zou, C. Yi, Y. Sun, Y. Cao, R. Yang, Y. Wei, Q. Guo, Y. Ke, M. Yu, Y. Jin, Y. Liu, Q. Ding, D. Di, L. Yang, G. Xing, H. Tian, C. Jin, F. Gao, R. H. Friend, J. Wang, and W. Huang, "Perovskite light-emitting diodes based on solution-processed self-organized multiple quantum wells," Nat. Photonics **10**(11), 699–704 (2016).
[18] H. Esmaielpour, V. R. Whiteside, S. Sourabh, G. E. Eperon, J. T. Precht, M. C. Beard, H. Lu, B. K. Durant, and I. R. Sellers, "Role of exciton binding energy on LO phonon broadening and polaron formation in $(Ba)_2PbI_4$ ruddlesdenpopper films," J. Phys. Chem. **124**, 9496 (2020).
[19] J. Even, L. Pedesseau, and C. Katan, "Understanding quantum confinement of charge carriers in layered 2D hybrid perovskites," ChemPhysChem **15**(17), 3733–3741 (2014).
[20] X. Wu, M. Tuan Trinh, D. Niesner, H. Zhu, Z. Norman, J. S. Owen, O. Yaffe, B. J. Kudisch, and X.-Y. Zhu, "Trap states in lead iodide perovskites," J. Am. Chem. Soc. **137**(5), 2089–2096 (2015).
[21] E. R. Dohner, E. T. Hoke, and H. I. Karunadasa, "Self-assembly of broadband white-light emitters," J. Am. Chem. Soc. **136**(5), 1718–1721 (2014).

[22]E. R. Dohner, A. Jaffe, L. R. Bradshaw, and H. I. Karunadasa, "Intrinsic white-light emission from layered hybrid perovskites," J. Am. Chem. Soc. **136**(38), 13154–13157 (2014).
[23]M. D. Smith and H. I. Karunadasa, "White-light emission from layered halide perovskites," Acc. Chem. Res. **51**(3), 619–627 (2018).
[24]H. Kim, M.-J. Choi, J. M. Suh, J. S. Han, S. G. Kim, Q. V. Le, S. Y. Kim, and H. W. Jang, "Quasi-2D halide perovskites for resistive switching devices with ON/OFF ratios above 109," NPG Asia Mater. **12**(1), 21 (2020).
[25]R. Li, C. Yi, R. Ge, W. Zou, L. Cheng, N. Wang, J. Wang, and W. Huang, "Room-temperature electroluminescence from two-dimensional lead halide perovskites," Appl. Phys. Lett. **109**(15), 151101 (2016).
[26]L. Ni, U. Huynh, A. Cheminal, T. H. Thomas, R. Shivanna, T. F. Hinrichsen, S. Ahmad, A. Sadhanala, and A. Rao, "Real-time observation of exciton–phonon coupling dynamics in self-assembled hybrid perovskite quantum wells," ACS Nano **11**(11), 10834–10843 (2017).
[27]J. V. Passarelli, D. J. Fairfield, N. A. Sather, M. P. Hendricks, H. Sai, C. L. Stern, and S. I. Stupp, "Enhanced out-of-plane conductivity and photovoltaic performance in n = 1 layered perovskites through organic cation design," J. Am. Chem. Soc. **140**(23), 7313–7323 (2018).
[28]D. Marongiu, M. Saba, F. Quochi, A. Mura, and G. Bongiovanni, "The role of excitons in 3D and 2D lead halide perovskites," J. Mater. Chem. C **7**, 12006–12018 (2019).
[29]V. Sarritzu, N. Sestu, D. Marongiu, X. Chang, Q. Wang, M. A. Loi, F. Quochi, M. Saba, A. Mura, and G. Bongiovanni, "Perovskite excitonics: Primary exciton creation and crossover from free carriers to a secondary exciton phase," Adv. Opt. Mater. **6**(3), 1700839 (2018).
[30]M. Saba, M. Cadelano, D. Marongiu, F. Chen, V. Sarritzu, N. Sestu, C. Figus, M. Aresti, R. Piras, A. Geddo Lehmann, C. Cannas, A. Musinu, F. Quochi, A. Mura, and G. Bongiovanni, "Correlated electron–hole plasma in organometal perovskites," Nat. Commun. **5**(1), 5049 (2014).
[31]K. Tvingstedt, O. Malinkiewicz, A. Baumann, C. Deibel, H. J. Snaith, V. Dyakonov, and H. J. Bolink, "Radiative efficiency of lead iodide based perovskite solar cells," Sci. Rep. **4**(1), 6071 (2014).
[32]D. B. Mitzi, K. Chondroudis, and C. R. Kagan, "Design, structure, and optical properties of organic–inorganic perovskites containing an oligothiophene chromophore," Inorg. Chem. **38**(26), 6246–6256 (1999).
[33]V. D'Innocenzo, G. Grancini, M. J. P. Alcocer, A. R. Srimath Kandada, S. D. Stranks, M. M. Lee, G. Lanzani, H. J. Snaith, and A. Petrozza, "Excitons versus free charges in organo-lead tri-halide perovskites," Nat. Commun. **5**(1), 3586 (2014).
[34]D. B. Mitzi, *Synthesis, Structure, and Properties of Organic-Inorganic Perovskites and Related Materials* (John Wiley & Sons, Ltd., 1999), pp. 1–121.
[35]K. Gauthron, J.-S. Lauret, L. Doyennette, G. Lanty, A. Al Choueiry, S. J. Zhang, A. Brehier, L. Largeau, O. Mauguin, J. Bloch, and E. Deleporte, "Optical spectroscopy of two-dimensional layered $(C_6H_5C_2H_4\text{-}NH_3)_2\text{-}PbI_4$ perovskite," Opt. Express **18**(6), 5912–5919 (2010).
[36]H. Jin, E. Debroye, M. Keshavarz, I. G. Scheblykin, M. B. J. Roeffaers, J. Hofkens, and J. A. Steele, "It's a trap! on the nature of localised states and charge trapping in lead halide perovskites," Mater. Horiz. **7**, 397–410 (2020).
[37]C. F. Klingshirn, *Semiconductor Optics* (Springer-Verlag Berlin Heidelberg, Berlin, 2012).
[38]S. Rana, K. Awasthi, S. S. Bhosale, E. W.-G. Diau, and N. Ohta, "Temperature-dependent electroabsorption and electrophotoluminescence and exciton binding energy in $MAPbBr_3$ perovskite quantum dots," J. Phys. Chem. C **123**(32), 19927–19937 (2019).
[39]M. Anni, A. Cretí, M. L. De Giorgi, and M. Lomascolo, "Local morphology effects on the photoluminescence properties of thin $CsPbBr_3$ nanocrystal films," Nanomaterials **11**(6), 1470 (2021).
[40]A. D. Wright, C. Verdi, R. L. Milot, G. E. Eperon, M. A. Pérez-Osorio, H. J. Snaith, F. Giustino, M. B. Johnston, and L. M. Herz, "Electron–phonon coupling in hybrid lead halide perovskites," Nat. Commun. **7**(1), 11755 (2016).
[41]X. Hong, T. Ishihara, and A. V. Nurmikko, "Dielectric confinement effect on excitons in PbI_4-based layered semiconductors," Phys. Rev. B **45**, 6961–6964 (1992).
[42]T. Fujita, Y. Sato, T. Kuitani, and T. Ishihara, "Tunable polariton absorption of distributed feedback microcavities at room temperature," Phys. Rev. B **57**, 12428–12434 (1998).
[43]M. Bokdam, T. Sander, A. Stroppa, S. Picozzi, D. D. Sarma, C. Franchini, and G. Kresse, "Role of polar phonons in the photo excited state of metal halide perovskites," Sci. Rep. **6**(1), 28618 (2016).
[44]P. Umari, E. Mosconi, and F. De Angelis, "Infrared dielectric screening determines the low exciton binding energy of metal-halide perovskites," J. Phys. Chem. Lett. **9**(3), 620–627 (2018).
[45]A. M. Soufiani, F. Huang, P. Reece, R. Sheng, A. Ho-Baillie, and M. A. Green, "Polaronic exciton binding energy in iodide and bromide organic-inorganic lead halide perovskites," Appl. Phys. Lett. **107**, 231902 (2015).
[46]M. Baranowski and P. Plochocka, "Excitons in metal-halide perovskites," Adv. Energy Mater. **10**(26), 1903659 (2020).
[47]S. Rudin, T. L. Reinecke, and B. Segall, "Temperature-dependent exciton linewidths in semiconductors," Phys. Rev. B **42**, 11218–11231 (1990).
[48]L. Malikova, W. Krystek, F. H. Pollak, N. Dai, A. Cavus, and M. C. Tamargo, "Temperature dependence of the direct gaps of ZnSe and $Zn_{0.56}Cd_{0.44}Se$," Phys. Rev. B **54**, 1819–1824 (1996).
[49]H. C. Woo, J. W. Choi, J. Shin, S.-H. Chin, H. A. Myung, and C.-L. Lee, "Temperature-dependent photoluminescence of $CH_3NH_3PbBr_3$ perovskite quantum dots and bulk counterparts," J. Phys. Chem. Lett. **9**(14), 4066–4074 (2018).
[50]M. C. Gélvez-Rueda, S. Peeters, P.-C. Wang, K. M. Felter, and F. C. Grozema, "Effect of structural defects and impurities on the excited state dynamics of 2D BA_2PbI_4 perovskite," Helv. Chim. Acta **103**(9), e2000121 (2020).